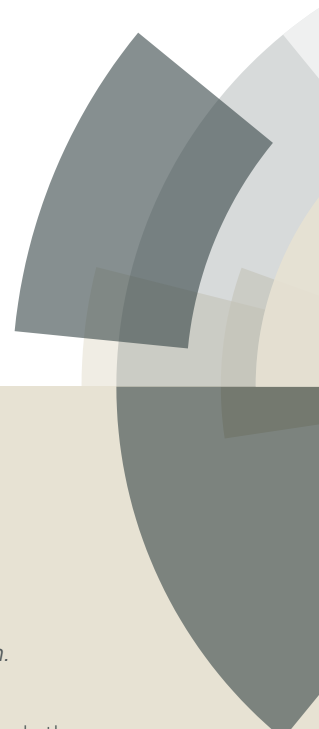


PCCP

Accepted Manuscript



This article can be cited before page numbers have been issued, to do this please use: F. Forato, S. Talebzadeh, N. Rousseau, J. Mévellec, B. Bujoli, D. A. Knight, C. Queffelec and B. Humbert, *Phys. Chem. Chem. Phys.*, 2019, DOI: 10.1039/C8CP07504B.



This is an Accepted Manuscript, which has been through the Royal Society of Chemistry peer review process and has been accepted for publication.

Accepted Manuscripts are published online shortly after acceptance, before technical editing, formatting and proof reading. Using this free service, authors can make their results available to the community, in citable form, before we publish the edited article. We will replace this Accepted Manuscript with the edited and formatted Advance Article as soon as it is available.

You can find more information about Accepted Manuscripts in the [author guidelines](#).

Please note that technical editing may introduce minor changes to the text and/or graphics, which may alter content. The journal's standard [Terms & Conditions](#) and the ethical guidelines, outlined in our [author and reviewer resource centre](#), still apply. In no event shall the Royal Society of Chemistry be held responsible for any errors or omissions in this Accepted Manuscript or any consequences arising from the use of any information it contains.

Journal Name

ARTICLE

Functionalized core-shell Ag@TiO₂ nanoparticles for enhanced Raman spectroscopy : a sensitive detection method for Cu(II) ions

Florian Forato,^a Somayeh Talebzadeh,^b Nicolas Rousseau,^c Jean-Yves Mevellec,^c Bruno Bujoli,^a D. Andrew Knight,^b Clémence Queffelec^{a*} and Bernard Humbert^{c*}

Received 00th January 20xx,
Accepted 00th January 20xx

DOI: 10.1039/x0xx00000x

www.rsc.org/

This paper demonstrates the use of Surface Plasmon Resonance of core-shell Ag@TiO₂ particles in SHINERS experiments. A copper(II) complex grafted onto Ag@TiO₂ surface was probed by Raman spectroscopy using resonance excitation profiles vs excitation wavelengths (514, 633 and 785 nm) to tune the Raman signals. Enhancement factors of the SHINERS assembly have been estimated and compared to the SERS effect of unmodified silver NPs colloidal dispersions. Finally, the grafting of the copper(II) complex onto Ag@TiO₂ was advantageously compared to the grafting onto Ag@SiO₂ shell.

Introduction

The study of core-shell metal nanoparticles (NPs) is an emerging field and has attracted attention especially in the field of photocatalysis,^{1–3} and a wealth of synthetic strategies are available for these materials.⁴ Principally, these synthetic strategies fall into two main categories: (a) a one-step preparation of core-shell nanoparticles involving simultaneous growth of noble metal nanoparticles and metal oxide shells, and (b) coating of previously prepared metal nanoparticles with a shell of metal oxide. This second approach often leads to improved monodispersity of the core-shell structures and is also attractive for the formation of non-centrosymmetric morphologies.^{5,6} Some examples of interesting shapes include yolk-shell⁷ Janus,⁸ flower-like⁹ and eccentric¹⁰ and many of these structures exhibit novel plasmonic properties. Metal oxides usually employed are silicon oxide^{11–14} although titanium or zirconium oxide have been employed as well.¹⁵ Regarding the metals, gold, copper and silver have been the most used, and silver has probably played the most important role in the development of plasmonics.¹⁶

Surface Plasmon Resonance (SPR) is an interesting characteristic of metal NPs which has been largely employed for surface enhanced spectroscopy,¹⁷ biological and chemical imaging,^{18,19} lithographic fabrication,^{20–22} and other applications.^{16,23,24} One of the major developments is Surface

Enhanced Raman Scattering (SERS) that can increase a Raman signal measurement by 10⁴ to 10¹⁰, and small molecules can be detected with small NPs or aggregates. In 2010, Li et al.²⁵ developed SHell-Isolated Nanoparticle-Enhanced Raman spectroscopy (SHINERS) in which the Raman amplification of the signal was provided by gold nanoparticles with an ultrathin silica or alumina shell. This core-shell prevented the aggregation of NPs without loss of the SPR effect. Since then, the SHINERS technique has been extended to others metals, (also including non-reactive shells) and has been employed for various applications.^{26–30} In this work, the binding of phosphonic acid-based organometallic complexes to core-shell Ag@TiO₂ nanoparticles is described and is compared to the silicon oxide shell analog. This paper demonstrates the importance of controlling the TiO₂ shell in SERS applications. Silver is known to possess an intense plasmon band,^{24,31} and is a relatively inexpensive metal. We decided to focus our attention towards Ag@TiO₂ NPs, in which the titania shell prevents oxidation of silver and allows the grafting of a bipyridine-based ligand bearing a phosphonic acid group through the formation of an ionic-covalent bond. The SPR of our SHINERS core-shell Ag@TiO₂ particles is used here to probe a copper(II) complex adsorbed onto the surface by Raman spectroscopy using plots of enhancement profiles vs excitation wavelengths. The best SHINERS effect for the copper(II) complex is observed with a low-focused power laser excitation at 633 nm, as the SHINERS effect is much weaker for example at 785 nm and at 514 nm. Specifically, for green excitation, the copper complex degraded after only a few seconds. This paper also compares enhancement factors of the SHINERS assembly with the SERS effect of unmodified silver NPs colloidal dispersions by using the enhanced Raman spectrum of the bipyridine skeleton. Finally, we demonstrate using the Raman signals, that the TiO₂ shell does not possess a direct chemical bonding interaction between Ag atoms and the bipyridine ligand. As copper is an important metal used in a wide variety of applications and its detection in aqueous and organic solvents is of interest, we have

^a Chimie Et Interdisciplinarité: Synthèse Analyse Modélisation (CEISAM), Université de Nantes, CNRS, UMR 6230, 2, rue de la Houssinière, BP 92208, 44322 Nantes Cedex 3, France. E-mail : clemence.queffelec@univ-nantes.fr

^b Chemistry Department, Florida Institute of Technology, 150 West University Boulevard, Melbourne, Florida, 32901, USA

^c Institut des Matériaux Jean Rouxel, CNRS-Université de Nantes, 2 rue de la Houssinière, B.P. 32229, 44322 Nantes Cedex 3, France. E-mail : Bernard.Humbert@cnsr-immn.fr

Electronic Supplementary Information (ESI) available: [Synthesis of nanomaterials, sample preparation for Raman, UV-vis spectra of Ag@SiO₂ and Ag@SiO₂@bpy-PA and TEM images, Raman spectrum at 633 nm of Ag@TiO₂@bpy-PA NPs at the millimolar and the micromolar concentration]. See DOI: 10.1039/x0xx00000x

investigated the possibility of copper ion detection using SERS by direct complexation with the N-N donor set of grafted bipyridine groups on SHINERS particles.

Material and methods

Starting materials.

All chemical reagents and solvent were purchased from commercial sources (Aldrich, Acros, SDS) and used as received. ^1H NMR spectra were recorded on Bruker Avance 300 MHz or 400 MHz spectrometers. Chemical shifts are reported (in parts per million) relative to internal tetramethylsilane (Me_4Si , $\delta = 0.00$ ppm) or referenced to the residual solvent. Silica gel (200-300 mesh) was used for flash chromatography. TLC plates were visualized by immersion in anisaldehyde or permanganate stain followed by heating.

The syntheses of the ligand bpy-PA and $\text{Ag}@\text{TiO}_2@\text{L}@\text{Cu}$ NPs have been reported previously.³²

RAMAN spectroscopy

Raman spectra were recorded using a microconfocal Raman inVia™ Reflex Renishaw device. The instrument was equipped with a double edge filter to eliminate the Rayleigh scattering, and a charged couple device (CCD) camera working at a temperature of 220 K and with a 1024 by 256 pixel array. Laser excitations used were 457.9, 488, 514.53, 632.82 and 785 nm wavelengths. The setup was composed of a confocal microscope that was equipped with an automated XYZ table. The spectral resolution achieved with the use of gratings of 2400, 1800 or 1200 grooves per millimetre was between 2 and 3.5 cm^{-1} according to the excitation wavelength. All the Raman characteristics (optical responses vs wavelength, vs polarisation, wavenumber accuracy, stability etc.) were calibrated based on previous methods.³³ The accuracy of the wavenumber, verified with the silicon Raman signal, was better than 0.5 cm^{-1} . The focused power of the laser beam was also checked for each wavelength to avoid any transformation or heating of the samples. Accordingly, the power was kept below $100\text{ }\mu\text{W}/\mu\text{m}^2$ and the magnitudes $\times 50$ and $\times 20$ of the objective (numerical aperture respectively of 0.75 and 0.35 and then a spot size of around respectively of 1.5 and $15\text{ }\mu\text{m}^2$) has been selected after a test list. The confocal mode was also sometimes used to select a smaller analyzed volume in the same irradiated volume and to record Raman spectra with the better lateral spatial resolution (around at $\lambda/2$) in order to check the heterogeneity of our films. The acquisition time was between 1 s and 30 s in order to obtain an enough signal-to noise ratio without damaging the samples.

For sample preparation, colloidal solutions were dropped onto silica slides under a flow of argon gas until water evaporation, approximately fifteen successive evaporations are needed in order to obtain a suitable amount.

Nanoparticle characterization

Nanoparticle morphology was investigated by transmission electron microscopy (TEM, 1230 Jeol) working at a voltage of

120 keV, using holey carbon-coated copper grids (300 mesh) to gain enough electronic contrast. View Article Online
DOI: 10.1039/C8CP07504B

UV-Vis absorption

UV-Vis absorption spectra were obtained on a 5000 CARY VARIAN spectrophotometer using water, or dichloromethane as the solvent for organic compounds.

Comparison of the enhancement of Raman signals

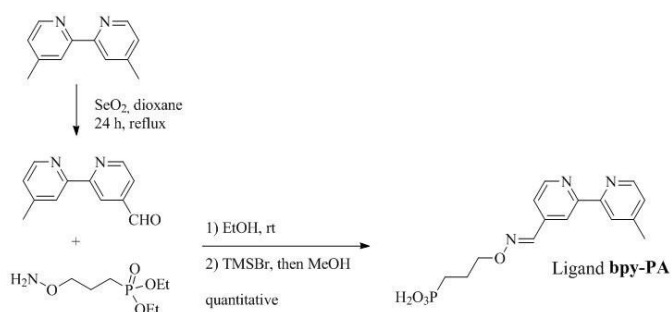
In order to estimate the enhancement factor of our SHINERS NPs and to test the lack of accessibility of bipyridine towards binding at the silver interface, our spectra were compared with SERS signals obtained with silver colloidal NPs in the presence of an aqueous solution of bipyridine (10^{-4} M).³⁴ The colloidal dispersion of silver NPs was synthesized by the usual method in aqueous medium by the reduction of AgNO_3 by NaBH_4 . The quasi spherical Ag NPs with a diameter around $14\text{ nm} \pm 7\text{ nm}$ was either deposited on a pure silica glass or used directly in suspension in contact with 2,2'-bipyridine solutions. Colloidal silver NPs were also functionalized by a self-assembly C_{12} spacer thiol monolayer (SAM) in order to have a protective layer between bipyridine molecules and silver NPs. Signal intensities allowed us to estimate the magnitude of enhanced factors of our shiners at the same wavelengths for the same quantity of bipyridine groups adsorbed per square nanometer.

Results and discussion

1. Synthesis of ligand bpy-PA

The 2,2'-bipyridine (bpy) ligand is ubiquitous in metal coordination chemistry and is able to coordinate to a large number of transition metal ions in solution usually with high binding constants. The wealth of different coordination geometries that bipyridine (bpy) metal complexes may adopt can give rise to different Raman spectral features. This has been exploited recently in the use of the bpy ligand in combination with Ag nanoparticles for the detection of a wide variety of metal ions in aqueous solution including Fe(II), Zn(II), Cu(II), Cd(II) and Cr(III). Rapid SERS analysis was achieved using a benchtop Raman spectrometer fitted with a 96-well microtitre plate.³⁵

We focused on the ligand bpy-PA for which the synthesis has previously been reported.³² Briefly, 4,4'-dimethyl-2,2'-bipyridine was functionalized with one aldehyde group^{36,37} that allowed attachment of the phosphonate tether bearing oxyamine end-groups ($\text{NH}_2\text{-O-(CH}_2\text{)}_3\text{-P(O)(OR)}_2$) in ethanol, via the formation of a stable O-alkyloxime bond (-C=N-O-). Then hydrolysis of the phosphonate esters using McKenna's method³⁸ afforded ligand bpy-PA in a good yield (Scheme 1, 19.2% over 5 steps).



Scheme 1. Synthesis of ligand bpy-PA

2. Synthesis of Ag@TiO₂@bpy-PA and characterization

It is important to point out that a titanium oxide shell was chosen over silicon oxide for two different reasons :

- We recently investigated the immobilization of a rhodium complex based on phosphonate-functionalized 2,2'-bipyridine on titanium oxide particles generated in situ. Successful immobilization of the catalysts on titanium oxide particles was demonstrated by different characterization techniques [³¹P magic angle spinning (MAS) NMR spectroscopy correlated with DFT calculations, X-ray photoelectron spectroscopy (XPS), and time-of-flight secondary-ion mass spectrometry (ToF-SIMS)].³⁹ We thus assumed the grafting would be similar in the case of Ag@TiO₂ and will ensure a strong binding between the ligand and the core-shell NPs.

- Silicon oxide shell usually leads to well-dispersed Ag@SiO₂ core-shell NPs. We synthesized Ag@SiO₂ NPs following an adapted procedure from literature^{40,41} and monodispersed NPs were obtained (Figure S1). Then the ligand was added to form Ag@SiO₂@bpy-PA NPs, and comparison of Ag@SiO₂, before and after grafting, demonstrated that the silica layer was partially destroyed and a high degree of silver NP aggregation appears to be present in the TEM images (Figure S2). We currently do not have an explanation for this phenomenon. However, for these reasons, Ag@TiO₂ was selected over Ag@SiO₂ for the SHINERS experiments.

The synthesis of silver NPs is quite straightforward and Ag NPs were obtained from the reduction of silver nitrate with hydrazine monohydrate to give a yellow coloured solution of stable Ag NPs and TiO₂ core-shell was then formed through the hydrolysis of titanium tetraisopropoxide (TTIP) in water.^{5,32} The Ag NPs were randomly distributed in the titania matrix and Ag@TiO₂ nanocomposites had a silver core diameter ca. 10-30 nm and the TiO₂ shell thickness was ca. 2-10 nm (Figure S3).

A bpy-PA solution in water was added to the Ag@TiO₂ NPs and left to stir overnight. The resulting Ag@TiO₂@bpy-PA nanocomposite was concentrated by cross-flow filtration, centrifuged, washed exhaustively with water to remove any unreacted phosphonic acid and redispersed in water.

3. Synthesis of Ag@TiO₂@bpy-PA-Cu(II) and characterization

Copper is an important metal used in a wide variety of applications and its detection in aqueous and organic solvents

is thus of interest. We first decided to look at copper(II) ions due to their high stability in water.

DOI: 10.1039/C8CP07504B

For the synthesis of Ag@TiO₂@bpy-PA-Cu(II), an aqueous copper(II) solution was added to Ag@TiO₂@bpy-PA suspension. (molar ratio Ag/Ti is around 0.06%).³² After 16 hours, Ag@TiO₂@bpy-PA-Cu(II) was obtained after centrifugation, allowing the formation of spherical nanoparticles. Dynamic light scattering (DLS) measurements were performed, but due to evolutive aggregation, their interpretation and simulations couldn't be used with confidence. As such, we chose to perform a statistical analysis of TEM images for the size determination of silver NPs in the Ag@TiO₂ nanocomposite.

Figure 1 shows a TEM image of Ag@TiO₂@bpy-PA-Cu(II) in which spherical nanoparticles are shown with an average diameter around 20 nm.

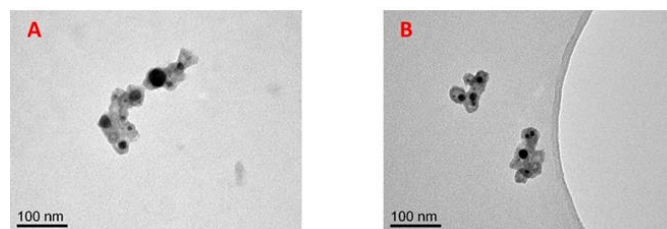


Figure 1. TEM images of a) Ag@TiO₂@bpy-PA b) Ag@TiO₂@bpy-PA-Cu(II) NPs

4. UV-Vis absorption spectroscopy

The formation of colloids was monitored by UV-vis absorption spectroscopy and a spectral comparison of unprotected Ag NPs, core-shell Ag@TiO₂, Ag@TiO₂@bpy-PA and Ag@TiO₂@bpy-PA-Cu(II) are shown in Figure 2. The plasmon band can clearly be seen in all four samples confirming the formation of nanoparticles. The peak maximum corresponding to the plasmon excitation of silver is around 405 nm.¹⁶ As expected with the encapsulation and the change of surrounding environment (dielectric shell around metal particles),⁴² the plasmonic band is red-shifted to 445 nm and decrease in intensity when coated with TiO₂. When ligand bpy-PA is attached to the Ag@TiO₂ NPs, the plasmon resonance band is further red-shifted to 450 nm. Upon coordination of metal ions to Ag@TiO₂@bpy-PA nanocomposites, the shape of the transmission spectrum is nearly unchanged. For copper(II), the spectrum displays a broadening of SPR band around 450 nm related to the plasmon resonance and some copper-complex electronic transitions can be observed in the near IR region.

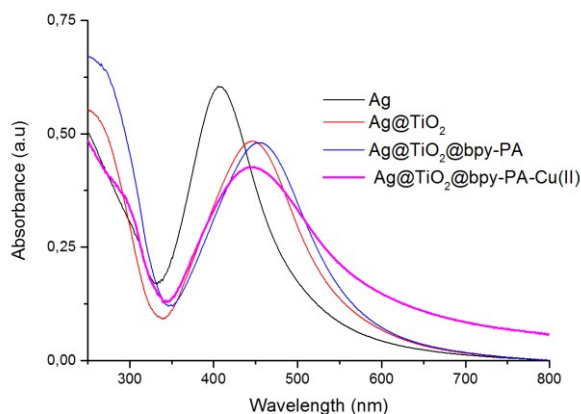


Figure 2: UV-vis spectra of Ag@TiO₂@bpy-PA-Cu(II) NPs; Arrows indicate the different excitation wavelength of Raman spectra, 514.53, 632.8 and 785 nm displayed in Figures 3 and 4.

5. Enhanced Raman Spectroscopic Study

5.1. Samples preparation for Raman spectroscopy

Backscattered Raman spectra of Ag@TiO₂@bpy-PA and Ag@TiO₂@bpy-PA@Cu(II) nanocomposites were recorded on films directly deposited from the colloidal solution onto pure silica glass slides. The percentage of coverage by the bpy-PA ligand onto core-shell NPs was tested during our Raman analyses. We grafted (i) around 400 bpy-PA per nm² (multilayer of bpy-PA around NPs) while using a millimolar aqueous solution of ligand or (ii) approximately one bpy-PA/nm² (submonolayer of bpy-PA on NPs) when using a micromolar aqueous solution of ligand.

Raman spectra were recorded for both concentrations and for the lowest concentration, the spectra were less noisy (Figure S4). Therefore, only results with the micromolar concentration are shown. It is important to point out that for detection, the

slides were dipped 5 min into the copper solutions, then dried before Raman characterization. DOI: 10.1039/C8CP07504B

5.2. Raman data for Ag@TiO₂@bpy-PA at 514 nm

To characterize the grafted complexes, Raman measurements were first performed with a laser excitation at 488 nm. Ag@TiO₂@bpy-PA was the first sample studied and was compared to a sample of the ligand grafted directly onto TiO₂ particles (TiO₂@bpy-PA). Mostly signals corresponding to the bipyridine skeleton were observed in the presence of Ag NPs and no signals were detected for TiO₂@bpy-PA, even with a laser power two hundred times higher. These results confirm that silver nanoparticles are required to enhance the signals of the ligand, suggesting as well that the amount of ligand bound to the TiO₂ surface is too low to be directly detected, on both concentrations tested. Moreover, after a few seconds, additional fluorescence signals were observed and the overall spectrum changed, suggesting a degradation of the sample under laser irradiation.

Therefore, the laser wavelength was changed to 514 nm. We first looked at adsorbed bipyridine molecules on rough silver electrodes (Figure 3A)⁴² or adsorbed bipyridine molecules with a thiol tether on colloidal silver nanoparticles (Figure 3B). As expected, the SERS effect of the bipyridine group is weaker with an organic spacer than the enhancement obtained using directly adsorbed bipyridine molecules on colloidal Ag NPs (Figure 3A) but these are always observed. The Raman spectrum of the Ag@TiO₂@bpy-PA film was thus recorded at 514 nm at a low focused laser power (ca. 100 μW per 5 μm²) in 1 second (Figure 3C) and then was compared to the two other samples described above to qualitatively assign the vibrational Raman scatterings.

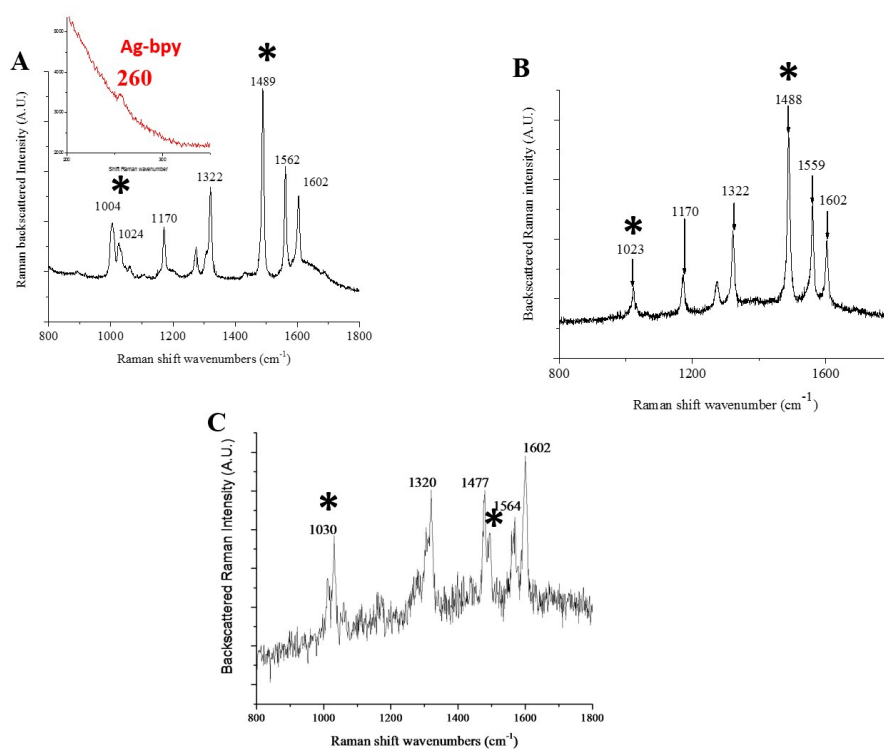


Figure 3 : (A) Raman spectrum of 2,2'-bipyridine at 10^{-4} M in a colloidal solution of Ag at 514 nm. In the insert, zoom on the range spectrum of 200 and 350 cm^{-1} showing a Ag-bpy band around 260 cm^{-1} ; (B) Raman spectrum of 2,2'-bipyridine with a thiol functionalized C-12 spacer at 10^{-4} M in a colloidal solution of Ag at 514 nm (C) Raman spectrum of Ag@TiO₂@bpy-PA (power density : 25 $\mu\text{W}\cdot\mu\text{m}^{-2}$) at 514 nm. The quantity adsorbed of bpy-PA is around the monolayer at the surface of Ag@TiO₂.

The spectrum of Ag@TiO₂@bpy-PA is dominated by the vibrational modes of the bipyridine unit and is very similar to that obtained using adsorbed bipyridine molecules with an organic thiol tether on colloidal Ag NPs (Figure 3B). By comparing recorded intensities of signals and focused power values at the same wavelength, the enhancement for Ag@TiO₂@bpy-PA may be estimated to be three orders of magnitude weaker than for colloidal Ag@bpy NPs. The SERS spectra display the active modes of bipyridine in five principal ranges (i) 1600-1560 cm^{-1} , modes involving C=C and C=N stretchings and possible in-plane CNH deformations; (ii) 1500-1450 cm^{-1} for C=C and C=N ring stretching and the CCH in-plane deformations; (iii) 1250-1150 cm^{-1} for CCH in-plane deformations weakly coupled with the ring stretching modes; (iv) 1100-980 cm^{-1} for ring breathing modes and (v) 300-200 cm^{-1} for possible Ag-N modes (insert in Figure 3A). This last range exhibits no signal for all Ag@TiO₂@bpy-PA samples, thus no bonds between the silver surface and bipyridine groups was observed.

5.3. Evaluation of the enhancement factor

The SERS enhancement factor of our core-shell Ag@TiO₂@bpy-PA NPs has been estimated in two different ways (for more details, see the Supporting Information):

(i) This factor may be expressed as the ratio $\{I(\text{sers intensity at one wavenumber}) / I(\text{usual raman at the same wavenumber})\}$, where both intensities are excited with the same incident power focused on the same area and the wavenumber corresponds to the characteristic Raman shift of the molecule. As the Raman profile is different between the conventional bipyridine fragments (not displayed here) and the SERS bipyridine fragments of our sample, the same wavenumber for both structures is not easy to choose. In our case, the signals around 1010 and 1490 cm^{-1} (Figure 3, peaks labels with stars) could be used for calculations. With the integrated intensities, we can claim then that the enhancement factor in our case is between 500 and 2×10^3 .

(ii) The factor may be estimated also by comparing Raman spectra obtained with our core-shell systems to the ones recorded with colloidal silver NPs interacting with bipyridine molecules. Profiles are in this case very similar and the enhancement factor may be evaluated by using different signals. Thus, our system is 10^{-3} to 10^{-4} less efficient than colloidal silver NPs and 10^{-2} to 10^{-3} less efficient than capped silver NPs by C12 long chains. (NB : with our calculation method, we could estimate the enhancement factor per bipyridine adsorbed on colloidal silver NPs by comparing their responses to the conventional Raman recorded with our device for the

2,2'-bipyridine without SERS, and the EF would be between 5×10^7 and 10^8 , which is consistent with data of literature).

5.4. Raman results at 633 nm

Because 514 nm is too high in energy resulting in some degradation of the material, we then recorded the spectrum of Ag@TiO₂@bpy-PA at 633 nm and we compared it to Ag@SiO₂@bpy-PA (Figure S4). With a low power laser, the spectrum of Ag@TiO₂@bpy-PA displayed bipyridine modes while for Ag@SiO₂@bpy-PA, the spectrum is more complicated and was evolving and degrading during acquisition. Some spectral feature of bipyridine can be observed with other peaks probably arising from the degradation of the bipyridine backbone. Besides, during acquisition, the peak corresponding to Ag-N bond could be observed around 250-260 cm^{-1} , confirming the result obtained by TEM.

Then, we compared spectra of Ag@TiO₂@bpy-PA and Ag@TiO₂@bpy-PA-Cu(II) (Figure 4). The signal at 230 cm^{-1} observed for Ag@TiO₂@bpy-PA-Cu(II) is representative of the Cu-N bond. As show in the Figure 4 inset, a small shift in the wavenumber values for the bipyridine modes could be observed, confirming that copper is coordinated to the bipyridine skeleton. In this case, we observed no Ag-N signals.

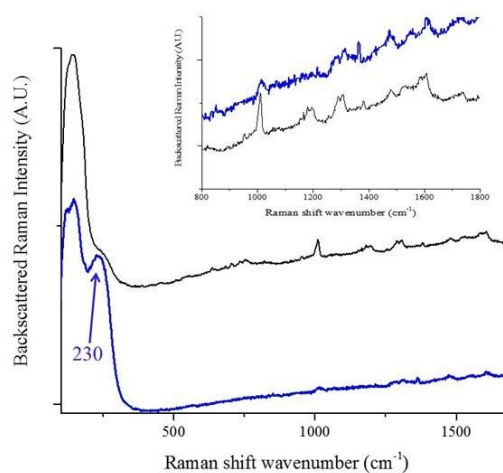


Figure 4 : Black : Raman spectrum of Ag@TiO₂@bpy-PA (power density : 75 $\mu\text{W}\cdot\mu\text{m}^{-2}$) at 633 nm. Blue : Raman spectrum of Ag@TiO₂@bpy-PA-Cu(II) (power density : 75 $\mu\text{W}\cdot\mu\text{m}^{-2}$) at 633 nm.

5.5. Comparison of Raman results at different wavelengths for Ag@TiO₂@bpy-PA-Cu(II)

Finally, spectra of Ag@TiO₂@bpy-PA-Cu(II) were compared at three different wavelengths, 514, 633 and 785 nm (Figure 5).

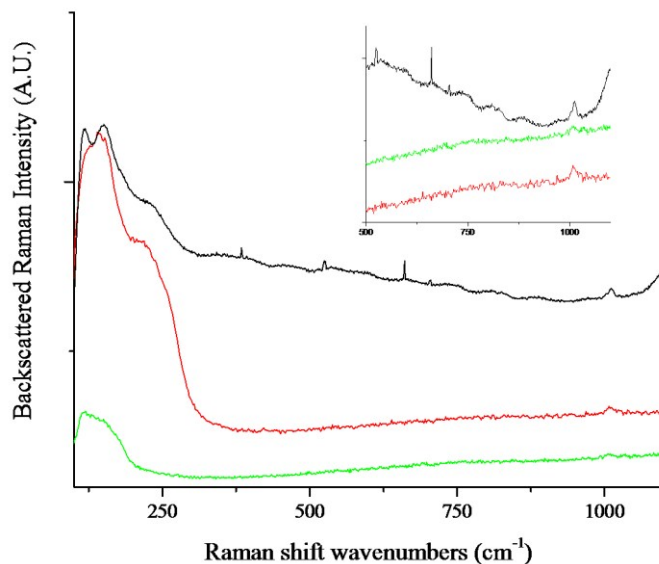


Figure 5: Comparison of Raman spectrum of Ag@TiO₂@bpy-PA-Cu(II). In green at 514 nm (power density : 50 $\mu\text{W}\cdot\mu\text{m}^{-2}$), in red at 633 nm (power density : 75 $\mu\text{W}\cdot\mu\text{m}^{-2}$) and in black at 785 nm (power density : 175 $\mu\text{W}\cdot\mu\text{m}^{-2}$).

At 633 and 785 nm, the Cu-N bond can be well observed. It is important to point out that at 785 nm, luminescence of silica originating from the glass slide caused interference with the samples between 1200 and 1800 cm^{-1} and it was clearly difficult to observe the bipyridine signals. At 514 nm, the sample was degrading after a few seconds. Thus, it seems from these results that 633 nm is the best compromise for the signal enhancement and sample stability.

Conclusion

In conclusion, we have developed a new SERS platform by using shell-isolated NPs capped by titanium oxide and functionalized by 2,2'-bipyridine bearing a phosphonic acid end-group. We demonstrated here that a titanium oxide (TiO₂) shell is able to minimize the problem encountered with an analogous silicon oxide shell and a phosphonic acid group. The SERS effect is demonstrated with an enhancement factor of 10^3 - 10^4 , i.e. 10^{-3} to 10^{-4} lower than the SERS signal obtained with an uncoated silver NP. Moreover, Shell Isolated Enhanced Raman Spectroscopy (SHINERS) was demonstrated for the copper(II) coordination complex. The efficiency was optimum with a 633 nm excitation. On this basis, this new platform will be investigated as a potential new analytical technique to detect

selectively copper ions in aqueous solutions at the picomolar level. The method might be straightforward, robust and applicable in harsh environments such as sea-water where the simple SERS method may be limiting. The ability of the sensor platform to be recycled and to selectively detect other metal ions will be included in future work.

Conflicts of interest

There are no conflicts to declare.

Acknowledgements

The authors acknowledge financial support from the "Centre National de la Recherche Scientifique" (CNRS) through the PICS COSMOCAT.

References

- 1 K. Awazu, M. Fujimaki, C. Rockstuhl, J. Tominaga, H. Murakami, Y. Ohki, N. Yoshida and T. Watanabe, A plasmonic photocatalyst consisting of silver nanoparticles embedded in titanium dioxide, *J. Am. Chem. Soc.*, 2008, **130**, 1676–1680.
- 2 P. Wang, B. Huang, X. Qin, X. Zhang, Y. Dai, J. Wei and M.-H. Whangbo, Ag@AgCl: A highly efficient and stable photocatalyst

- active under visible light, *Angew. Chem.-Int. Ed.*, 2008, **47**, 7931–7933.
- 3 X.-C. Ma, Y. Dai, L. Yu and B.-B. Huang, Energy transfer in plasmonic photocatalytic composites, *Light-Sci. Appl.*, 2016, **5**, e16017.
 - 4 Z. W. Seh, S. Liu and M.-Y. Han, Titania-Coated Metal Nanostructures, *Chem. – Asian J.*, 2012, **7**, 2174–2184.
 - 5 H. Sakai, T. Kanda, H. Shibata, T. Ohkubo and M. Abe, Preparation of Highly Dispersed Core/Shell-type Titania Nanocapsules Containing a Single Ag Nanoparticle, *J. Am. Chem. Soc.*, 2006, **128**, 4944–4945.
 - 6 K. S. Mayya, D. I. Gittins and F. Caruso, Gold–Titania Core–Shell Nanoparticles by Polyelectrolyte Complexation with a Titania Precursor, *Chem. Mater.*, 2001, **13**, 3833–3836.
 - 7 R. Güttel, M. Paul and F. Schüth, Activity improvement of gold yolk–shell catalysts for CO oxidation by doping with TiO₂, *Catal. Sci. Technol.*, 2011, **1**, 65–68.
 - 8 Z. W. Seh, S. Liu, M. Low, S.-Y. Zhang, Z. Liu, A. Mlayah and M.-Y. Han, Janus Au-TiO₂ Photocatalysts with Strong Localization of Plasmonic Near-Fields for Efficient Visible-Light Hydrogen Generation, *Adv. Mater.*, 2012, **24**, 2310–2314.
 - 9 N. Zhang, S. Liu, X. Fu and Y.-J. Xu, Synthesis of M@TiO₂ (M = Au, Pd, Pt) Core–Shell Nanocomposites with Tunable Photoreactivity, *J. Phys. Chem. C*, 2011, **115**, 9136–9145.
 - 10 D. D. Lekeufack, A. Brioude, A. Mouti, J. G. Alazun, P. Stadelmann, A. W. Coleman and P. Miele, Core–shell Au@(TiO₂, SiO₂) nanoparticles with tunable morphology, *Chem. Commun.*, 2010, **46**, 4544–4546.
 - 11 Y. Lu, Y. D. Yin, Z. Y. Li and Y. N. Xia, Synthesis and self-assembly of Au@SiO₂ core-shell colloids, *Nano Lett.*, 2002, **2**, 785–788.
 - 12 Y. Lu, Y. D. Yin, B. T. Mayers and Y. N. Xia, Modifying the surface properties of superparamagnetic iron oxide nanoparticles through a sol-gel approach, *Nano Lett.*, 2002, **2**, 183–186.
 - 13 M. A. Hossain, J. Park, D. Yoo, Y.-K. Baek, Y. Kim, S. H. Kim and D. Lee, Surface plasmonic effects on dye-sensitized solar cells by SiO₂-encapsulated Ag nanoparticles, *Curr. Appl. Phys.*, 2016, **16**, 397–403.
 - 14 L. M. Liz-Marzan, M. Giersig and P. Mulvaney, Synthesis of nanosized gold-silica core-shell particles, *Langmuir*, 1996, **12**, 4329–4335.
 - 15 R. T. Tom, A. S. Nair, N. Singh, M. Aslam, C. L. Nagendra, R. Philip, K. Vijayamohan and T. Pradeep, Freely dispersible Au@TiO₂, Au@ZrO₂, Ag@TiO₂, and Ag@ZrO₂ core-shell nanoparticles: One-step synthesis, characterization, spectroscopy, and optical limiting properties, *Langmuir*, 2003, **19**, 3439–3445.
 - 16 M. Rycenga, C. M. Cobley, J. Zeng, W. Li, C. H. Moran, Q. Zhang, D. Qin and Y. Xia, Controlling the Synthesis and Assembly of Silver Nanostructures for Plasmonic Applications, *Chem. Rev.*, 2011, **111**, 3669–3712.
 - 17 S. M. Nie and S. R. Emery, Probing single molecules and single nanoparticles by surface-enhanced Raman scattering, *Science*, 1997, **275**, 1102–1106.
 - 18 L. S. Jung, C. T. Campbell, T. M. Chinowsky, M. N. Mar and S. S. Yee, Quantitative interpretation of the response of surface plasmon resonance sensors to adsorbed films, *Langmuir*, 1998, **14**, 5636–5648.
 - 19 J. M. Brockman, B. P. Nelson and R. M. Corn, Surface plasmon resonance imaging measurements of ultrathin organic films, *Annu. Rev. Phys. Chem.*, 2000, **51**, 41–63.
 - 20 Z. Xie, W. Yu, T. Wang, H. Zhang, Y. Fu, H. Liu, F. Li, Z. Lu and Q. Sun, Plasmonic Nanolithography: A Review, *Plasmonics*, 2011, **6**, 565–580.
 - 21 W. Srituravanich, N. Fang, C. Sun, Q. Luo and X. Zhang, Plasmonic nanolithography, *Nano Lett.*, 2004, **4**, 1085–1088.
 - 22 A. Bouvrée, A. D'Orlando, T. Makiabadi, S. Martin, G. Louarn, J. Y. Mevellec and B. Humbert, Nanostructured and nanopatterned gold surfaces: application to the surface-enhanced Raman spectroscopy, *Gold Bull.*, 2013, **46**, 283–290.
 - 23 K. A. Willets and R. P. Van Duyne, in *Annual Review of Physical Chemistry*, 2007, vol. 58, pp. 267–297.
 - 24 K. L. Kelly, E. Coronado, L. L. Zhao and G. C. Schatz, The optical properties of metal nanoparticles: The influence of size, shape, and dielectric environment, *J. Phys. Chem. B*, 2003, **107**, 668–677.
 - 25 J. F. Li, Y. F. Huang, Y. Ding, Z. L. Yang, S. B. Li, X. S. Zhou, F. R. Fan, W. Zhang, Z. Y. Zhou, D. Y. Wu, B. Ren, Z. L. Wang and Z. Q. Tian, Shell-isolated nanoparticle-enhanced Raman spectroscopy, *Nature*, 2010, **464**, 392–395.
 - 26 S. Guan, O. Donovan-Sheppard, C. Reece, D. J. Willock, A. J. Wain and G. A. Attard, Structure Sensitivity in Catalytic Hydrogenation at Platinum Surfaces Measured by Shell-Isolated Nanoparticle Enhanced Raman Spectroscopy (SHINERS), *Acs Catal.*, 2016, **6**, 1822–1832.
 - 27 J. F. Li, X. D. Tian, S. B. Li, J. R. Anema, Z. L. Yang, Y. Ding, Y. F. Wu, Y. M. Zeng, Q. Z. Chen, B. Ren, Z. L. Wang and Z. Q. Tian, Surface analysis using shell-isolated nanoparticle-enhanced Raman spectroscopy, *Nat. Protoc.*, 2013, **8**, 52–65.
 - 28 J.-F. Li, J. R. Anema, T. Wandlowski and Z.-Q. Tian, Dielectric shell isolated and graphene shell isolated nanoparticle enhanced Raman spectroscopies and their applications, *Chem. Soc. Rev.*, 2015, **44**, 8399–8409.
 - 29 C. Zheng, W. Shao, S. K. Paidi, B. Han, T. Fu, D. Wu, L. Bi, W. Xu, Z. Fan and I. Barman, Pursuing shell-isolated nanoparticle-enhanced Raman spectroscopy (SHINERS) for concomitant detection of breast lesions and microcalcifications, *Nanoscale*, 2015, **7**, 16960–16968.
 - 30 K. G. Schmitt, R. Schmidt, H. F. von-Horsten, G. Vazhenin and A. A. Gewirth, 3-Mercapto-1-Propanesulfonate for Cu Electrodeposition Studied by in Situ Shell-Isolated Nanoparticle-Enhanced Raman Spectroscopy, Density Functional Theory Calculations, and Cyclic Voltammetry, *J. Phys. Chem. C*, 2015, **119**, 23453–23462.
 - 31 C. Burda, X. B. Chen, R. Narayanan and M. A. El-Sayed, Chemistry and properties of nanocrystals of different shapes, *Chem. Rev.*, 2005, **105**, 1025–1102.
 - 32 F. Forato, S. Talebzadeh, B. Bujoli, C. Queffelec, S. A. Trammell and D. A. Knight, Core-Shell Ag@TiO₂ Nanocomposites for Low-Power Blue Laser Enhanced Copper(I) Catalyzed Ullmann Coupling, *Chemistryselect*, 2017, **2**, 769–773.
 - 33 J. Grausem, B. Humbert, M. Spajer, D. Courjon, A. Burneau and J. Oswald, Near-field Raman spectroscopy, *J. Raman Spectrosc.*, 1999, **30**, 833–840.
 - 34 A. De Bonis, G. Compagnini, R. S. Cataliotti and G. Marletta, Adsorption-induced conformational transition in 2,2'-bipyridine on silver surfaces: a surface-enhanced Raman scattering study, *J. Raman Spectrosc.*, 1999, **30**, 1067–1071.
 - 35 J. Docherty, S. Mabbott, W. E. Smith, J. Reglinski, K. Faulds, C. Davidson and D. Graham, Determination of metal ion concentrations by SERS using 2,2'-bipyridyl complexes, *Analyst*, 2015, **140**, 6538–6543.
 - 36 C. Busche, P. Comba, A. Mayboroda and H. Wadepohl, Novel Ru-II Complexes with Bispidine-Based Bridging Ligands: Luminescence Sensing and Photocatalytic Properties, *Eur. J. Inorg. Chem.*, 2010, 1295–1302.

- 37 K. E. Berg, A. Tran, M. K. Raymond, M. Abrahamsson, J. Wolny, S. Redon, M. Andersson, L. C. Sun, S. Styring, L. Hammarstrom, H. Toftlund and B. Akermark, Covalently linked ruthenium(II)-manganese(II) complexes: Distance dependence of quenching and electron transfer, *Eur. J. Inorg. Chem.*, 2001, 1019–1029.
- 38 C. E. McKenna, M. T. Higa, N. H. Cheung and M. C. McKenna, Facile Dealkylation of Phosphonic Acid Dialkyl Esters by Bromotrimethylsilane, *Tetrahedron Lett.*, 1977, 155–158.
- 39 F. Forato, A. Belhboub, J. Monot, M. Petit, R. Benoit, V. Saroukian, F. Fayon, D. Jacquemin, C. Queffelec and B. Bujoli, Phosphonate-Mediated Immobilization of Rhodium/Bipyridine Hydrogenation Catalysts, *Chem. – Eur. J.*, 2018, **24**, 2457–2465.
- 40 J. E. Lee, S. Bera, Y. S. Choi and W. I. Lee, Size-dependent plasmonic effects of M and M@SiO₂ (M = Au or Ag) deposited on TiO₂ in photocatalytic oxidation reactions, *Appl. Catal. B-Environ.*, 2017, **214**, 15–22.
- 41 W. Stober, A. Fink and E. Bohn, Controlled Growth of Monodisperse Silica Spheres in Micron Size Range, *J. Colloid Interface Sci.*, 1968, **26**, 62-.
- 42 A. Taleb, C. Petit and M. P. Pileni, Synthesis of Highly Monodisperse Silver Nanoparticles from AOT Reverse Micelles: A Way to 2D and 3D Self-Organization, *Chem. Mater.*, 1997, **9**, 950–959.

View Article Online
DOI: 10.1039/C8CP07504B

TOC

A shell-isolated nanoparticle enhanced surface Raman technique for detection of copper(II)

